1.1 Historical sketch of alloys development

Materials design and development have the paramount importance in various fields of science and engineering application i.e., structural, transportation, aerospace, energy, medical, etc. The metals and their alloys played a fundamental role in every phase of human civilization all through the history [1]. Alloying was the precise gift, humankind got from nature, when arsenical bronze (alloy of Cu and As) was accidentally discovered in around 3000 BC. Bronze alloy of Cu and Sn was the first alloy prepared by the human civilization in 2500 BC during the period termed as Bronze Age [2–4]. From the early 20^{th} century, the industrial demand for newer materials increased drastically, which encouraged the development of various material for specific applications at affordable prices. This gives a breakthrough in the history of materials with the development of various grade of steels, Al-alloys and Ti-alloys, amorphous alloys, and superalloys, which boosted industrial productivity [5]. The development of various materials with the time is displayed in Figure 1.1. Various novel alloys were developed from bronze ages to native elements (Cu, Ag, Au, and Fe) [6], through binary alloys (Fe-C, and Cu-Zn) [7, 8], ternary alloys (Fe-Cr-Mn) [9, 10] and quaternary alloys (Fe-Mn-Al-C) [11, 12] to multiple element alloys.

Among all those alloy development, steels have the utmost importance in numerous applications from the iron age [5]. Since the discovery of iron, there have been lots of steels in the alloy world i.e., mild steel, stainless steel [13], dual-phase steel [14], low density steel [15], maraging steel [16], tool steel [17], etc., which have been used in many engineering applications. Initially carbon steel was synthesized by adding charcoal directly to wrought iron during melting [18]. This was mainly used in refineries and petrochemical plants for piping and valves because of its low cost. This carbon steel can be easily corroded in oil and gas atmosphere i.e., CO_2 and H_2S because of high carbon content. The stainless steel (Fe-Cr-C) was subsequently developed, which

showed better corrosion resistance as compared to carbon steel [20]. However, these steels lack mechanical

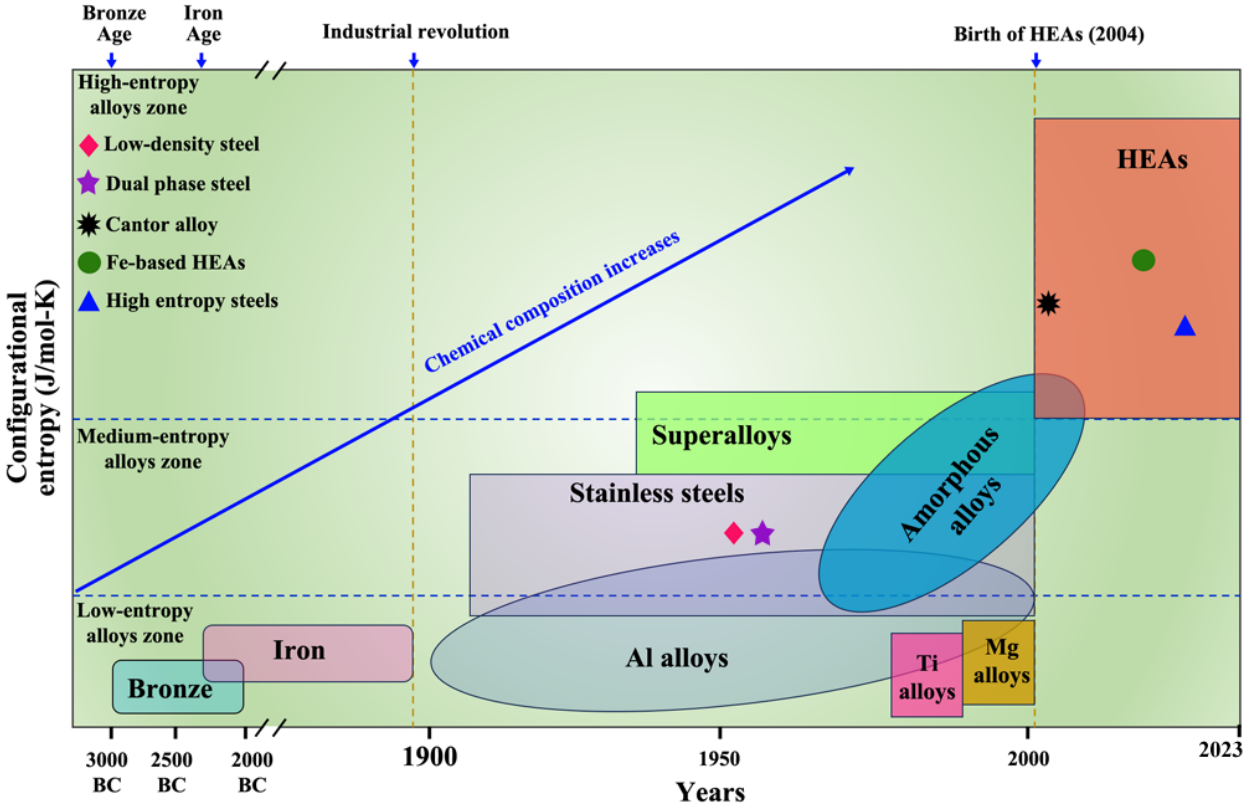

Figure 1.1: Development of various material with the time [19].

strength i.e., tensile yield strength (YS) at room temperature [21]. The duplex (ferritic-austenitic microstructure) stainless steel which exhibits higher tensile yield strength and excellent corrosion resistance as compared to other stainless steel was later developed [21]. However, duplex stainless steels formed the hard intermetallics (α′ (alpha prime) and σ (sigma)) at elevated temperature ranges of 300 °C to 500 °C, and 550 °C and 950 °C, respectively, which deteriorated the toughness and hot-corrosion resistance of the duplex steels [22]. The low-density steel was also developed in the same timeline as the duplex steel, which is shown in Figure 1.1. The lightweight Fe-Mn-Al-C and Fe-Mn-Al-Si-C steel have been explored for excellent mechanical properties and corrosion

resistance. However, these alloys have a high elastic modulus, which makes the alloy stiff and not possible to have the malleability [22, 23].

Since the bronze age, alloy development strategies have been focused on one principal element and the addition of one or more elements in minor quantity to achieve the desired properties for various applications. The classical physical metallurgy principles limit the compositional space to design the alloy [24]. Multicomponent alloys were first studied by Frank Karl-Archard in the year 1788. However, such research work was not carried forward, because the fact that multicomponent mixture fabricated by casting route mostly contains intermetallics and are brittle [24].

1.2 Historical background of HEAs

In 2004, after the report of multicomponent HEAs by Cantor and Yeh independently, the conventional alloy design concept changed and the novel concept of high entropy alloys was advocated containing at least five principal elements (with the individual element ranging from 5 to 35 at. %) [25, 26]. They all were in an equimolar or nearly equimolar quantity, which has high configurational entropy [27] and helps forming the disordered single-phase solid solution with BCC [21, 28, 29], FCC [26, 30, 31], and HCP [32–34] structure. The development of HEAs was classified on the basis of elements are 3d transition metals (Cr, Mn, Fe, Co, Ni, etc.) [35], refractory HEAs (W, Ta, Hf, Nb, etc) [36], and low-density elements (Mg, Al, Ca, Ti, etc) [37]. Cantor et al., [26] designed and fabricated an equiatomic CrMnCoFeNi HEA, with multiprincipal element. The alloy exhibits an FCC structure after the solidifications of arc-melted sample, and showed the good mechanical properties. Few of its properties are completely diverse from FCC metals. Lots of studied are done on Cantor alloy, by substituting one of the elements by Al, Ti, Mo, and Cu, etc., for better structural and functional properties [35]. Senkov et al. [38] designed and prepared the

WNbMoTa and WNbMoTaV HEA by vacuum arc melting (VAM). These alloys have formed a single-phase BCC structure and possessing excellent thermal stability up to 1600 ℃. The alloys have formed the single-phase despite having several constituents due to the four core effects of HEAs [38]. The hardness was found to be 4.4 GPa and 5.2 GPa for WNbMoTa and WNbMoTaV HEA, respectively, which is greater than the individual elements due to the solid solution strengthening [38]. The light weight MgMnAlZnCu HEA was prepared using the vacuum induction melting, which formed the HCP as the major phase along with the Al-Mn quasicrystal as secondary phase. The alloy showed the good hardness (4.2 GPa - 4.5 GPa) and compression strength (428 MPa - 450 MPa) at room temperature, but the poor compressive strains of 3.29% to 5.53% [39]. This alloy has good strength but poor ductility due to the formation of brittle secondary phase [39].

The non-equiatomic HEAs have expanded the compositional space and added more flexibilities to tune the structural and functional properties [40]. These non-equiatomic HEAs can be grouped into various classes: eutectic [41–44], element-based [45–47], precipitation strengthened [48–50], interstitial HEAs [51–53], TRIP and TWIP HEAs [54, 55], high entropy intermetallics [56–58], and high entropy steels [59, 60]. Among all the non-equiatomic HEAs, the Fe-based HEAs have shown unique microstructure, and excellent structural and functional properties [61, 62]. The class of Fe-based HEAs started with the fabrication of $Fe_{40}Mn_{27}Ni_{26}Co_5Cr_2$ [31], and $Fe_{40}Mn_{40}Co_{10}Cr_{10}$ [63] via vacuum arc melting leading to single-phase FCC structure with a good synergy of strength and ductility.

Raabe et al. [59] proposed the concept of high entropy steel, which is basically a Fe-based HEAs with carbon as an interstitial element [60]. Based on concept many such alloys were explored, showing good strength and ductility e.g., $Fe_{40.4}Ni_{11.3}Mn_{34.8}Al_{7.5}Cr_6$ [31],

$Fe_{40}Mn_{40}Co_{10}Cr_{10}$ [63], and $Cr_{20}Mn_{10}Fe_{35}Ni_{35}$ [64]. High entropy steel materials attracted the attention of materials community because, it has strength like steel and have many features like high entropy alloys. So, one can expect excellent mechanical and functional properties as well as compositional vastness in high entropy steel. Figure 1.1 shows the development of the Fe-based HEAs and high entropy steel, which is marked in green circle and blue triangle, respectively.

1.3 Core-effect of High Entropy Alloys

The HEAs are different from conventional alloys as the compositional space is complex but they may form the solid solution because of the hypotheses proposed by Yeh et al. [25], due to high entropy, sluggish diffusion, and lattice distortion. In addition, the cocktail effect is proposed by Ranganathan [65], appears to be effective in HEAs. These four core effects are discussed in details in following subsection.

1.3.1 High entropy effect

The most important core effect is high entropy effect, which helps to form a random solid solution rather than a complex compound. Based on the physical metallurgy concept it is anticipated that many intermetallics would form with multicomponent systems. However, experimental evidence of solid solution formation was reported in many multicomponent systems [66]. Yeh et al. [25] theorised that the high configurational entropy stabilizes the formation of solid solution rather than complex compounds. The configurational entropy of a system is calculated by Boltzmann's thermodynamics principle, as per the following equation,

$$\Delta S_{conf} = \mathrm{k} \ln w \tag{1.1}$$

where, k = Boltzmann's constant, and w = number of different means of arranging the atoms in the lattice. The ideal configurational entropy for an n component system, in which the X_i is the mole fraction of i^{th} element, is given as:

$$\Delta S_{conf} = -\mathrm{R}\sum_{i=1}^{n} X_i \ln X_i \tag{1.2}$$

where, R is the universal gas constant (8.314 J/K-mole). It may be noted that configurational entropy is not the only factor for phase formation in HEAs. Enthalpy of mixing also plays an important role here as high enthalpy of mixing results in phase separation and high negative enthalpy gives rise to intermetallic compound [67]. Subsequently, to form a stabilized random solid solution the configurational entropy should be very high and the enthalpy of mixing should be very small positive value [38].

1.3.2 Sluggish diffusion effect

The kinetics and phase transformation concept in the high entropy alloys was proposed by Yeh et al. [25]. In HEAs, the atomic diffusion of elements becomes sluggish due to varying atomic size, which slows down phase transformation. It leads to slower grain growth, reduced coarsening rate, evolution of fine precipitates, and increased recrystallization temperature [25]. New phase formation is restricted due to the sluggish diffusion effect as the movement of atoms is hindered [68, 69].

1.3.3 Severe lattice distortion

The solid sphere schematic model is shown in Figure 1.2, which shows the level of distortions in the structures of pure metals, binary alloys, and high entropy alloys [70]. Thus whole-solute matrix in the HEAs consists of atoms with different atomic size, and this makes the lattice severely

distorted [71]. In addition to different atomic size, the different crystal structures and atomic bonding energies among asymmetrical neighbouring atoms aid to the lattice distortion [72, 73]. The effect will cause the scattering of electrons and photons, which affects the electrical and thermal conductivity in HEAs [74, 75].

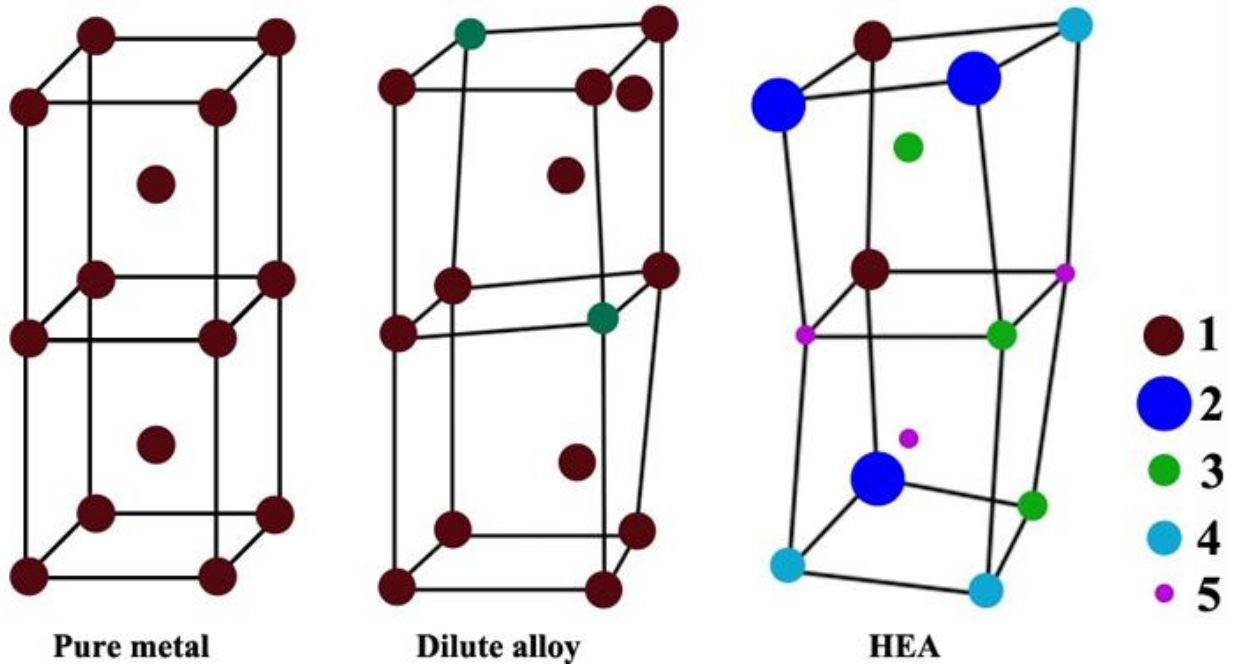

Figure 1.2: The lattice distortion in pure metals (BCC), binary alloys, and HEAs are shown schematic [76].

1.3.4 Cocktail effect

This effect was discussed by Ranganathan in the article "Alloyed pleasure: Multimetallic cocktails" [65]. The cocktail effect extended to highlight the synergistic effect on multicomponent alloy systems to achieve excellent properties that cannot be explained by the conventional rule of mixture [70, 77]. It's also proposed that the HEAs get the unusual and better than the average properties due to the mixed effect of all the constituent elements, much similar to a cocktail drink [36, 78]. Yeh et al. [79, 80] showed the cocktail effect by adding the Al element in the $Al_xCoCrCuFeAl$ alloy system by varying Al content from 0-35 at. %, which leads to a phase

transformation from an FCC structure to FCC + BCC to BCC. Due to the presence of dual-phase, higher strength was achieved. The summary of the four core effects is displayed in Figure 1.3.

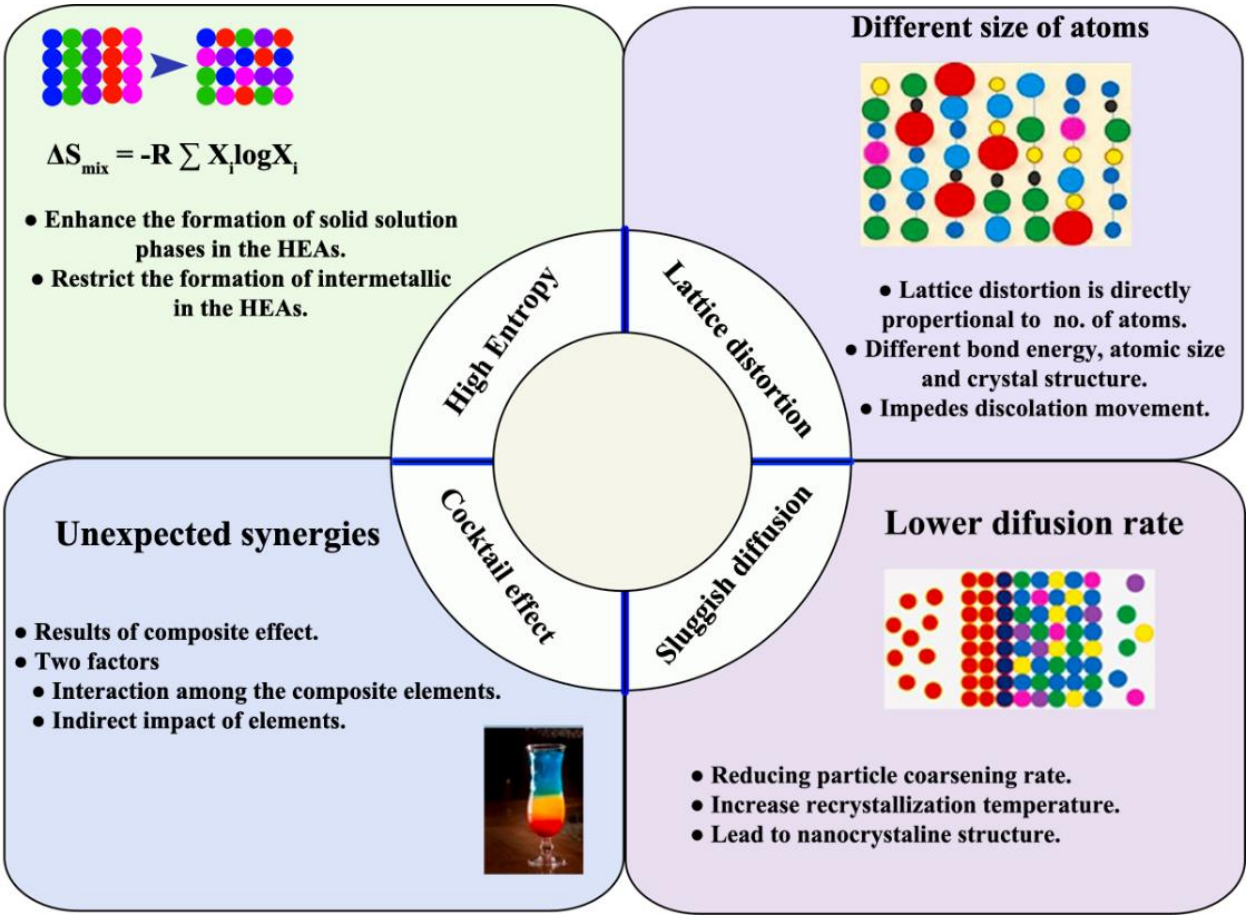

Figure 1.3: Summary of the four distinct core effects of the HEAs [19].

1.4 Phase selection by parametric approach and CALPHAD

1.4.1 Parametric approach

The classical Hume-Rothery rule for the formation of substitutional solid solution in the conventional alloy state that the crystal structure of the constituent alloying element needs to be same, they should have similar atomic size (within 15 %), valence electron concentration, and electronegativity. However, the Hume-Rothery rule is modified for HEAs to predict the solid

solution formation [81]. Zhang et al. [82], proposed some useful criteria for phase formation in high entropy alloys; those are mixing enthalpy (ΔH_{mix}), configurational entropy (ΔS_{conf}), and element radii mismatch (δ), electronegativity difference (Δχ), and valence electron concentration (VEC). The configurational entropy (J/mol-K) is discussed earlier in the section 1.3.1. The mixing enthalpy (kJ/mol) of the high entropy alloy is calculated using the following equation [83]

$$\Delta H_{mix} = \sum_{i=1, i \neq j}^{n} \Omega_{ij} C_i C_j \tag{1.3}$$

where, C_i and C_j are atomic percents of the i^{th} and j^{th} elements, Ω_{ij} = regular solution interaction parameter between i^{th} and j^{th} element, which is $\Omega_{ij} = 4\Delta H_{ij}^{mix}$, ΔH_{ij}^{mix} is the binary mixing enthalpy, which is calculated using Miedema's semi-empirical model [84, 85] and given as:

$$\Delta H_{mix}^{ij} = \frac{V_i^{2/3}}{(n_{ws}^{-\frac{1}{3}})_{avg}} \left[-P(\Delta\phi)^2 + Q\left(\Delta n_{ws}^{-\frac{1}{3}}\right)^2\right] \tag{1.4}$$

$$(n_{ws}^{-1/3})_{avg} = \frac{1}{2}\left[\frac{1}{(n_{ws}^{i})^{1/3} + (n_{ws}^{j})^{1/3}}\right] \tag{1.5}$$

where, P and Q = empirical constant, V = molar volume, ϕ = work function, n_{ws} = constituent electron density, (Δϕ) = electronegativity difference, and $(n_{ws})_{ave}$ = difference in the electron density at the boundary of the Wigner-Sietz cell of pure metals. The values of the above-mentioned parameters of the elements used in the alloy design are listed in Table 1.1.

The atomic size mismatch (%) for the HEAs [86] is given as:

$$\delta = 100\sqrt{\sum_{i=1}^{n} C_i\left\{1 - \frac{r_i}{\bar{r}}\right\}^2} \tag{1.6}$$

where, C_i and r_i = atomic concentration and atomic radius of the ith elements, $\bar{r}$ = mean atomic radii, and n = number of elements in the multicomponent alloys. The solid solution forming criteria in the HEAs was studied and analysed by Zhang et al. [82] and Guo et al. [83], which stated that solid solution forms when $-22 \leq \Delta H_{mix} \leq 7$, $11 \leq \Delta S_{conf} \leq 19.5$ and $0 \leq \delta \leq 8.5$. Figure 1.4 depicts the effect of these parameters on phase formation in HEAs [82].

Table 1.1: The value of the parameters used to calculate the binary enthalpy (ΔH_{mix}^{ij}) [85]

Elements	**ϕ**	**$(n_{ws})^{1/3}$**	**$(V)^{2/3}$**
Fe	4.93	1.77	3.7
Mn	4.45	1.61	3.8
Ni	5.20	1.75	3.5
Cr	4.65	1.73	3.7
Ti	3.65	1.47	4.8
Al	4.20	1.39	4.6
Si	4.70	1.50	4.2
C	6.20	1.90	1.8

Yang and Zhang [82, 87] proposed a new dimensionless parameter omega (**Ω**) which combines the effect of entropy and enthalpy for solid solution formation in HEAs

$$\Omega = \frac{T_m \Delta S_{conf}}{|\Delta H_{mix}|} \tag{1.7}$$

where, T_m = melting point of the HEAs. The ΔS_{conf} and ΔH_{mix} was discussed earlier in this section. They observed that the $\Omega \geq 1$, is the criteria to form the solid solution in the HEAs. When $\Omega<1$, effect of enthalpy predominates and tends to form intermetallic. They also correlate the effect of δ and Ω parameters in the Figure 1.5. Valence electron concentration is another critical parameter to

predict the BCC or FCC or both in the HEAs, which is proposed by Guo et al. [88–90]. VEC can be calculated using following formulae [90, 91]:

$$VEC = \sum_{i=1}^{n} C_i(VEC)_i \tag{1.8}$$

where, $(VEC)_i$ = VEC for the i^{th} element. According to him the BCC phase formed when VEC < 6.87, FCC phase when VEC ≥ 8 and both when VEC coexist in between.

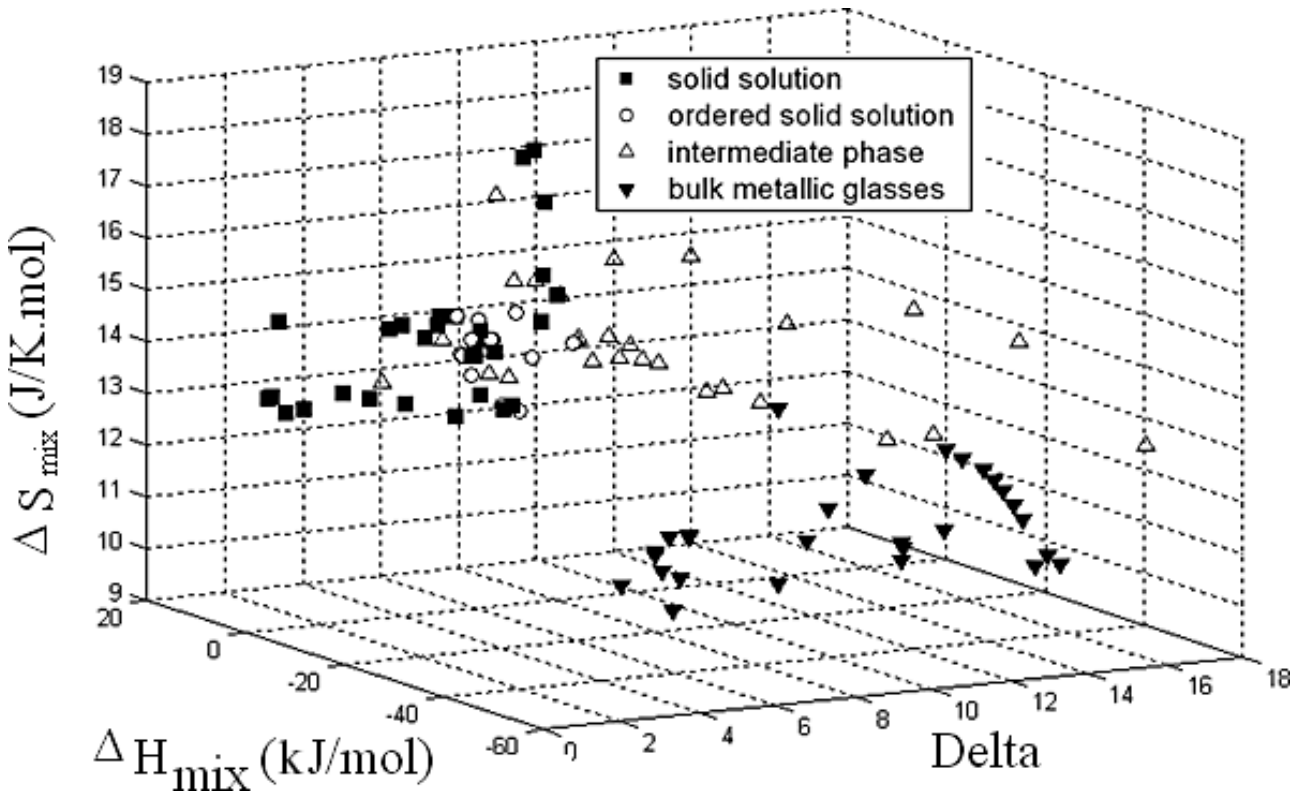

Figure 1.4: The effect of configurational entropy, mixing enthalpy and atomic mismatch on the phase formation of the multicomponent HEAs [2].

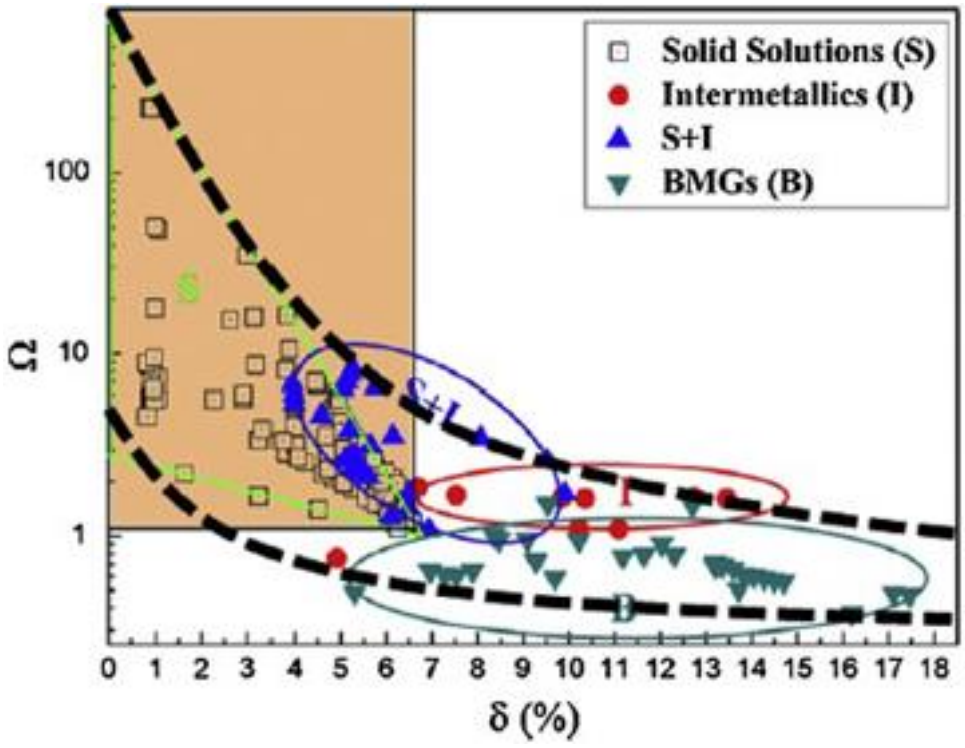

Figure 1.5: Relationship between δ and Ω parameters for the multiprincipal alloys. Solid solution (S) indicates that the multiprincipal alloys only form solid solutions. Intermetallics (I) infers that the alloy consisting of majorly intermetallic phase. S+I imply that the alloy composed of solid solution along with intermetallic as precipitates. BMGs demonstrates that the alloy have the amorphous phase (completely) [19].

1.4.2 CALPHAD modelling

In 1970, Larry Kaufman introduced a methodology CALPHAD, which stands for calculation of phase diagram. CALPHAD method is a thermodynamic computational tool that gives Gibb's free energy of different phase, which is a function of temperature and composition for binary and ternary alloy systems based on the experimental and theoretical results [92]. This tool is used for detailed analysis of binary, ternary, quaternary, and multicomponent alloy composition and provides the phase equilibrium, transition temperature, phase fraction, and phase chemistry [93, 94]. This method enables the development of thermodynamics and property databases to obtain the phase diagram of higher order systems based on data available of lower order systems [95].

This database has been extended to predict the phase formation in HEA systems [96, 97]. The predicted phase evaluated from CALPHAD approach, was corelated with the experimental results of non-equiatomic $Fe_xMn_{62-x}Ni_{30}Co_6Cr_2$ HEAs, where x = 22 to 42 at. %. The predicted phases from CALPHAD (TCFE7 database) are FCC and BCC phase with sigma as precipitates. The experiment findings showed that the alloys were formed the single-phase FCC solid solution after the annealing at 1473 K for 2 h, followed by water quenching. The work showed that the predictive capability of the CALPHAD approach for non-equiatomic HEAs with experimental findings are very well corelated [98]. The CALPHAD approach for predicting the phases in HEAs are useful tool for designing the HEAs [98].

1.5 High Entropy Steels and Fe-based HEAs

1.5.1 Synthesis

The high entropy steel and Fe-based HEAs are commonly prepared using liquid and solid-state processing. Coating deposition and additive manufacturing methods can also be used for preparing high entropy steel and Fe-based HEAs. Vacuum arc melting (VAM) and vacuum induction melting (VIM) are two major liquid state synthesis methods. The VAM uses an arc to generate a high temperature [99] whereas vacuum induction melting uses eddy current for melting the sample [100]. The HEAs prepared using these methods usually exhibit heterogenous solid solution with phase segregation, coarse grain, and dendritic and inter-dendritic microstructure, resulting in inferior mechanical properties. Evaporation of low-melting elements during melting is another drawback in vacuum arc melting process. Fe-based HEAs and high entropy steel fabricated using VAM and VIM have the coarse grain microstructure with average grain size more than 75 μm. Usually, these methods are followed by secondary treatments i.e., homogenisation, annealing and rolling to refine the grain size, which enhances the mechanical properties [101–104]. Secondary

treatment can also avoid unnecessary carbide formation and distribution, which affect the martensite nucleation and growth, and grains recrystallization in high entropy steel [105]. The Mn containing Fe-based HEAs and high entropy steel synthesised using the VAM, requires extra Mn addition to compensate for the Mn evaporation during melting, which may affect the alloy chemistry [106].

These inadequacies of the liquid metallurgical route can be easily overcome by the solid-state processing route, which provides more homogeneous and refined microstructures favourable for superior mechanical and functional properties [107]. This process mainly involves mechanical alloying (MA) of the elemental powders undergoing repeated cold-welding and fracturing of powder particles during milling [108]. First prepared alloy through mechanical alloying is oxide dispersion strengthened (ODS) alloy [109], afterwards this technique is used to prepare a variety of materials, like solid solution [110], amorphous [111], nanocomposite [112], and intermetallics [113], etc. In addition, this can expand the solid solubility limit in alloys, even in non-miscible alloys [114]. The large-scale production of powder sample is easily done by attritor mills, planetary ball mills, vibratory mills, and shaker mills. Milled powder is further densified by sintering methods (pressure less sintering, vacuum hot press, microwave, and spark plasma sintering) to produce desired shape and size of samples, which may not require further machining and sectioning process [115]. Spark plasma sintering (SPS) is a novel approach for sintering metallic and ceramic powders with the application of pressure and temperature simultaneously, which densifies the sample at a rapid rate and avoids unavoidable grain coarsening [116]. The sample consolidated by SPS can effectively retain the nanocrystalline nature [117]. $Fe_{35}Mn_{10}Cr_{20}Ni_{35}C_{1.2}$ high entropy steel synthesised by mechanical alloying followed by spark plasma sintering have achieved a relative density of 99.5 % with fine nanosized precipitates and matrix grain size of 0.7

μm [64]. The same composition alloy prepared by casting has tens/hundreds of micron sized grain which is much higher than the nanocrystalline grain structure prepared by powder metallurgy route [118, 119].

Additive manufacturing is a novel synthesis technique that works on the principle of layer-by-layer depositions of powder as a starting material to build the bulk samples. This technique can easily produce complex and intricate geometrical parts by using 3D printing or rapid prototyping, which can avoid the finishing processes of removing and cutting [120]. Based upon the working principle, they are classified into different methods i.e., selective laser melting (SLM), laser power bed fusion (L-PBF), and electron beam melting (EBM) [121]. $Fe_{40}Mn_{20}Co_{20}Cr_{15}Si_5$ prepared using LPBF, formed a single phase FCC structure. It is due to the layer by layer processing which gives rise to heat accumulation and thermal cycling. Absence of thermal cycling effect during the liquid metallurgy route leads to the formation of different phases even in same alloy chemistry [122]. However, it was also reported that the Fe-based HEAs and high entropy steel prepared using additive manufacturing had defects like voids and cracks which resulted in sudden failure during service [123, 124].

HEAs thin film and coatings have been extensively used in surface engineering applications due to their high mechanical properties, wear, and corrosion resistance in extreme environments. The thin film of the HEA material is mainly synthesized using laser cladding, thermal and cold spraying, laser deposition and plasma cladding, magnetron sputtering and vacuum arc deposition [125, 126]. Bao et al., [127] prepared the thin film of Fe-based $Fe_4CoCrNiB_{0.2}Mo_x$ (x = 0, 0.5, 1) HEAs by laser cladding on the Q235 substrate, which was well-developed without any defects, and the bonding between the cladding layer and the substrate was excellent. The morphology of the layer perpendicular to the interface and near the surface changed from cellular to columnar

grains and dendritic. This thin film of Fe-based HEAs showed a very high hardness of 7.2 GPa [127]. Figure 1.6 summarizes the various synthesis routes with some salient points and their microstructures formed in the high entropy steel and Fe-based HEAs.

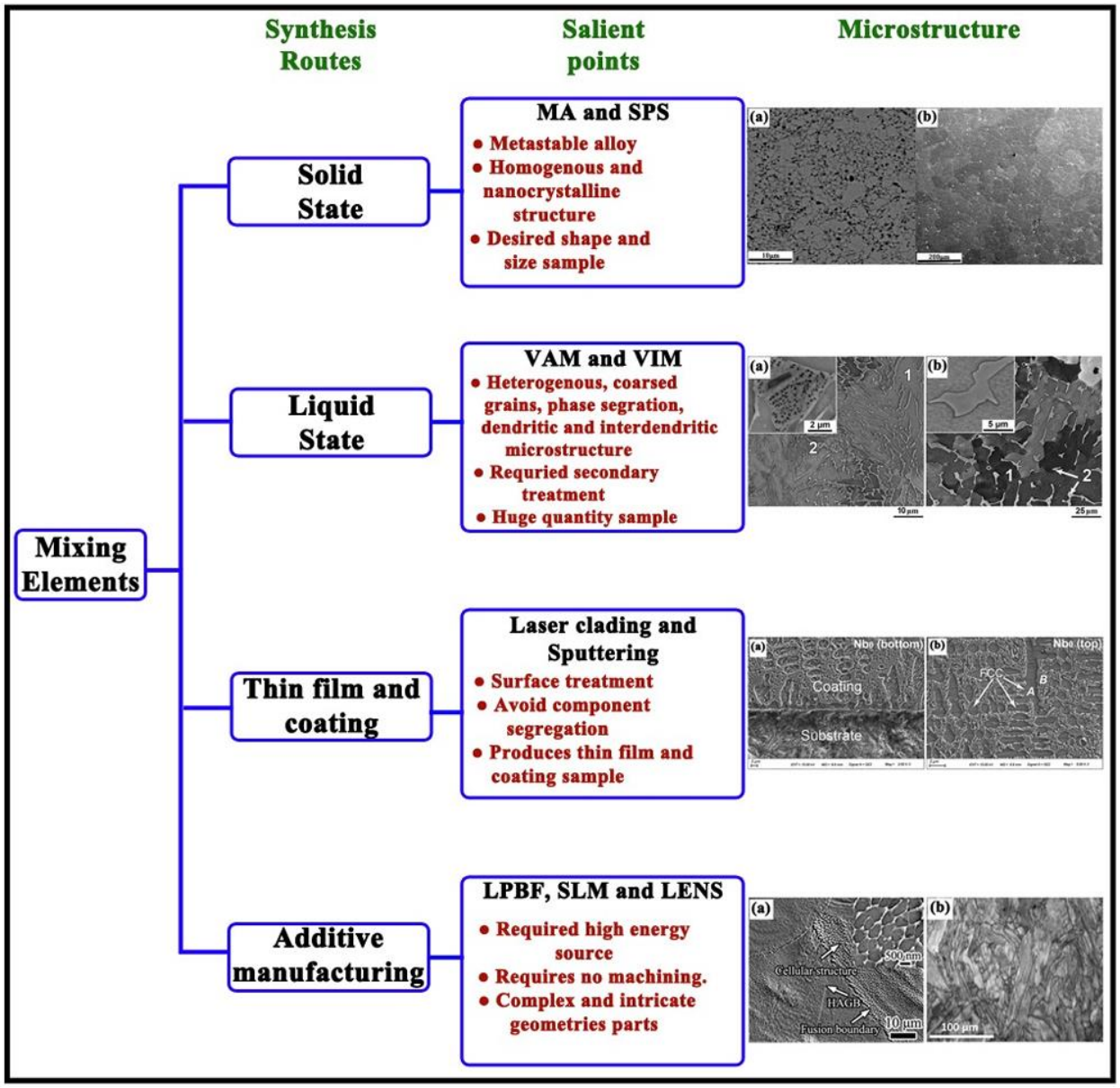

Figure 1.6: Summary of the various synthesis routes and its microstructures formed in the high entropy steels and Fe-based HEAs [64, 101, 122, 128, 129].

1.5.2 Structures

High entropy steel and Fe-based HEAs consists of major FCC or BCC phase or both similar to HEAs [130]. It can also form minor intermetallic phase and nanocrystalline precipitates. The structures of these alloys mostly depend upon the constituent elements, their composition as well as the processing routes [125].

Single phase structure is a rare event in high entropy alloy although the concept is based on single phase solid solution. But in Fe based high entropy alloy, due to its non-equiatomic nature, it can form single phase alloy or at least BCC/FCC as major phase. Kucuk et al. [131] synthesized the $Fe_{26.7}Ni_{26.7}Ga_{15.6}Mn_{20}Si_{11}$ HEA through the suction casting, which exhibited the single-phase BCC structure with lattice parameter close to 0.287 nm. Wang et al. [31] synthesized $Fe_{40.4}Ni_{11.3}Mn_{34.8}Al_{7.5}Cr_6C_x$ high entropy steel (x = 0, 0.07, 0.16, 0.3, 0.55 and 1.1 at. %) through the VAM, which exhibited single-phase FCC structure. $Fe_{60}Cr_{10}Mn_{10}Co_{10}Ni_{10}$ Fe-based HEA processed by VIM has also a single-phase FCC structure with a lattice parameter of 0.358 nm [132]. Kim et al. [133] fabricated the $V_{10}Cr_{15}Mn_5Fe_{35}Co_{10}Ni_{25}$ HEA through VIM, with the single-phase FCC structure.

Fe-based $(Fe_{40}Mn_{25}Cr_{20}Ni_{15})_{100-x}Al_x$ (x = 0–14 at. %) HEAs prepared using the VAM, displayed dual-phase structure mainly consisting of FCC and BCC/B2 [101]. As the Al content increased, the phase transformed from FCC and BCC to BCC and B2 structure [101]. $Fe_{50}Mn_{30}Co_{10}Cr_{10}$ HEA formed the FCC and HCP dual-phase structure after the gas atomization followed by SPS [119]. The dual-phase structure alloy showed the better properties as compared to the single-phase structure alloy [113].

HEAs with the formation of intermetallic compounds as secondary phases or precipitates i.e., γ' (gamma prime) [134], σ (sigma) [57], Laves [135], carbides [136], silicides [137], etc are essential in terms of structural and functional properties. These precipitates play a crucial role in enhancing the mechanical properties of the Fe-based HEAs and high entropy steel at room temperature and high temperature [138]. Fe-based FeNiCrMnAlTi HEAs showed the dual-phase structure mainly consisting of FCC and gamma prime (γ') along with η and $L2_1$ precipitates after the as-cast and homogenized samples. It was stated that the η precipitates formed with higher Al/Ti ratio and $L2_1$ precipitates with lower Al/Ti ratio [139]. A high entropy steel $(Fe_{35}Mn_{10}Cr_{20}Ni_{35})_{98.8}C_{1.2}$ has the single-phase FCC structure with M_7C_3 nanoprecipitates of size 100-200 nm after SPS [60]. The alloy showed a high yield strength of 1200 MPa with excellent ductility above 50 % [64].

1.5.3 Thermal stability

The structural material used for high-temperature applications ought to have phase stability at higher temperatures for better mechanical properties. Therefore, it is of paramount importance to establish the thermal stability of these high entropy steels and Fe-based HEAs to ascertain two aspects i.e., phase transformation and the retention of nanosized structure. HEAs prepared using the nonequilibrium processing routes like MA and sputtering, form metastable structures, which may further transform into other structures at elevated temperatures [140]. Although, HEAs synthesised by liquid metallurgy routes are less susceptible to phase transformation, they may form precipitates or secondary phase after annealing [141]. $Fe_{(64-x)}Mn_xNi_{27.7}Co_{5.6}Cr_{2.3}$ prepared using VAM, formed dual-phase structure. This alloy showed good thermal stability up to the 1300 ℃ due to the sluggish diffusion effect [142]. The Fe-based HEAs have the single-phase solid solution after the VIM, and do not reveal any exothermic or endothermic phase transformation peaks up to

melting point (~1250 °C) in DSC thermogram. These alloys showed a very stable FCC phase [102]. The dual-phase structure of BCC (major) and FCC was formed in $Fe_{25}Ni_{25}Co_{25}Ti_{15}Al_{10}$ HEA after the MA, and it transformed to FCC (major) and BCC after the SPS [143]. The various investigations on the thermal stability of the reported high entropy steel, Fe-based HEAs and non-equiatomic HEAs prepared through various processing routes are mentioned in Table 1.2.

Table 1.2: Thermal stability of the high entropy steels, Fe-based HEAs and non-equiatomic HEAs.

Alloys	**Synthesis route**	**Phases formed**	**DSC/Annealing treatment**	**Phase transformation**	**Ref.**
$Fe_{42}Mn_{20}Ni_{30}Co_6Cr_2$, $Fe_{37}Mn_{25}Ni_{30}Co_6Cr_2$, and $Fe_{32}Mn_{30}Ni_{30}Co_6Cr_2$	VIM	FCC	DSC was done from 25 °C to 1300 °C	No phase transformation	[98]
$Fe_{40}Mn_{27}Ni_{26}Co_5Cr_2$	VIM	FCC	DSC was done from 25 °C to 1250 °C	No phase transformation	[102]
$Fe_{27}Mn_{27}Ni_{27}Co_{11.5}Cr_7Nb_{0.08}C_{0.5}$, and $Fe_{29}Mn_{11.5}Ni_{29}Co_{16}Cr_{14.5}$	Centrifugal casting	FCC	DTA was done from 25 °C to 1400 °C	No phase transformation	[144]
$CoCrFeMn_{0.5}NiTi_{0.5}$	MA	BCC	700 °C, 1 h	FCC	[145]
$Al_{0.4}CoFeNiSi_x$ (x = 0.1 – 0.5, at. %)	MA	FCC + BCC + Si	Annealed in the temperature range of 300–600 °C	FCC + BCC + $CoFe_2O_4$	[146]

$Fe_{49.5}Mn_{29.7}Co_{9.9}Cr_{9.9}C_1$	VIM	FCC	Annealed at 650 °C, 800 °C, and 900 °C for 1 h then water quenched	FCC + HCP (at 900 °C)	[147]
$Fe_{40}Cr_{25}Ni_{15}Al_{15}Co_5$	VIM	BCC and B2	DSC was done from 25 °C to 1000 °C	No phase transformation	[148]
$Fe_{36}Mn_{21}Cr_{18}Ni_{15}Al_{10}$	VAM	Two BCC	Annealed at 1200 °C for 1 h	No phase transformation	[149]
$Fe_{64-x}Mn_xNi_{27.7}Co_{5.6}Cr_{2.3}$ (x = 21, 24, 27, 34, 38, at. %)	VAM	FCC	DSC was done up to 1300 °C	No phase transformation observed	[98]
$Al_{1.5}CrFeMnTi$	VAM	BCC + $L2_1$ + C14 Laves phase	Annealed at 750 °C and 850 °C for 168 h	BCC + $L2_1$ + C14 Laves phase	[150]

1.6 Properties

High entropy steel and Fe-based HEAs have shown excellent mechanical and functional properties, therefore they are taken as potential candidates for a wide range of applications i.e., structural, high-temperature, wear-resistant, and biomaterials. These excellent properties arise due to the unique microstructural and structural features of the high entropy steels and Fe-based HEAs. This section addresses various properties of such alloys including mechanical, wear, and functional properties.

1.6.1 Mechanical properties

Mechanical properties mainly cover hardness, elastic modulus, yield strength, ultimate strength, and elongation. Hardness measurements at different length scales ranging from Vickers hardness to instrumented micro and nanoindentation have been employed for high entropy steel and Fe-based HEAs. The alloys prepared using the powder metallurgy route show higher hardness as compared to alloy produced via melting route for similar compositional alloys [115]. Similarly, dual-phase HEAs have shown higher hardness as compared to single-phase HEAs [1]. The dual-phase (BCC and B2) structured $Fe_{34}Cr_{34}Ni_{14}Al_{14}Co_4$ HEA, prepared by VAM, shows ultimate strength and ductility of 2638 MPa and 40.6 %, respectively [151]. $(FeNi)_{67}Cr_{15}Mn_{10}Al_{8-x}Ti_x$ HEAs were focussed on dual-phase (FCC and γ') microstructure along with η and $L2_1$ as precipitates, to achieve the ultimate strength up to 1247 MPa with 22 % ductility. The excellent mechanical properties are credited to strain hardening and precipitation strengthening in the alloys [139]. Wei et al. [152] studied the effect of C and Mo on the mechanical properties of $Fe_{40}Mn_{40}Co_{10}Cr_{10}$ high entropy steel. The yield strength increases from 240 to 560 MPa by the addition of C and Mo (up to 1 wt. %). They also observed that the several strengthening mechanisms were activated due to the addition of C and Mo, which further improved the work-hardening rate followed by large plasticity. The investigation of the mechanical properties in $Fe_{40.4}Mn_{34.8}Ni_{11.3}Al_{7.5}Cr_6$ high entropy steel with varying carbon atomic percent was systematically done by Stepanov et al. [30]. The strength and the ductility of the high entropy steel increased up to 1.1 at. % of carbon and decreased with the carbon content (up to 4 at. %) [31]. Raabe et al., [60] prepared the FeMnAlC and FeMnAlSiC high entropy steel via VAM and merely focussed on FCC phase formation along with precipitates. This alloy showed a good combination of tensile strength up to 1000 MPa with ductility above 90 % due to the strain hardening and solid

solution strengthening [60]. Figure 1.7(a) shows where the high entropy steel in terms of ultimate tensile strength and elongation as compared to conventional alloys and other HEAs. High entropy steel usually shows average strength but excelled well in terms of ductility. Dual-phase structure in Fe-based HEAs show exceptional yield strength as well as reasonable amount of ductility, as illustrated in Figure 1.7(b).

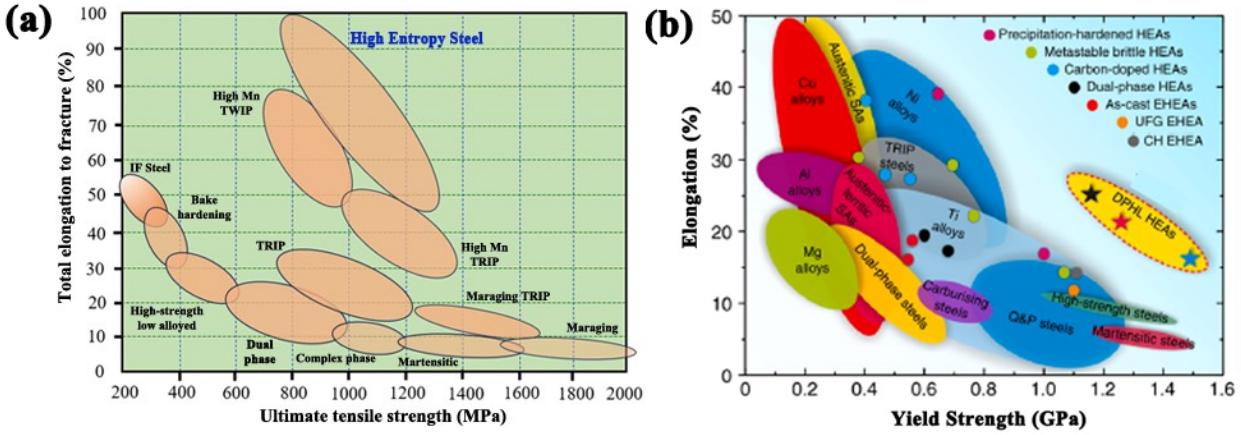

Figure 1.7: (a) Total elongation to fracture vs ultimate tensile strength of different types of steels and high entropy steels [60]; (b) Yield strength vs elongation of various conventional alloys and non-equiatomic HEAs [153].

Some of the Fe-based HEAs and high entropy steels, and their mechanical properties are tabulated in Table 1.3. The alloys are prepared using various techniques i.e., VAM, MA + SPS, etc. Usually, alloys prepared using powder metallurgy route give superior strength. Depending on various synthesis method and composition, they form various phases i.e., single phase, dual-phase and with precipitates. The dual-phase with precipitates exhibits higher strength.

Table 1.3: Alloy composition, phases formed, and mechanical properties of various high entropy steels, Fe-based HEAs, and conventional steel prepared using different synthesis routes.

Alloy composition	Synthesis route	Phases formed	Ultimate strength (MPa)	Strain (%)	Ref.
$Fe_{49.85}Cr_{10.03}Mn_{10.03}Co_{10.03}Ni_{10.03}Al_{10.03}$	VAM	FCC + BCC	636	30	[154]
$Fe_{37.06}Ni_{30.47}Mn_{12.44}Cr_{12.01}Al_{4.01}Ti_{4.01}$	VAM	FCC	922	30	[155]
$(Fe_{40}Ni_{30}Cr_{20}Al_{10})_{100-x}Ti_x$ (x = 0, 2, 4, 6, and 8)	VAM	FCC + BCC	723-1309	3-32	[156]
$Fe_{64-x}Mn_xNi_{27.7}Co_{5.6}Cr_{2.3}$ (x = 21, 24, 27, 34, 38, at. %)	VAM	FCC	380-420	50-60	[142]
$Co_{25.4}Cr_{15}Fe_{37.9}Mn_{3.5}Ni_{16.8}Si_{1.4}$	AM	FCC with CoCr nanoparticle	500	63	[157]
$Fe_{36}Mn_{21}Cr_{18}Ni_{15}Al_{10}$, $Fe_{36}Co_{21}Cr_{18}Ni_{15}Al_{10}$, $Fe_{35}Mn_{20}Cr_{17}Ni_{12}Al_{12}Ti_4$, and $Fe_{35}Co_{20}Cr_{17}Ni_{12}Al_{12}Ti_4$	VAM	FCC, BCC, B2 with $L2_1$	250-1420	26-40	[158]
$Fe_{44.12}Ni_{18}Mn_{12.98}Cr_{10.94}Al_{9.64}V_{4.32}$	VAM	BCC, FCC and B2	1000	11-17	[159]
$Fe_{40}Mn_{27}Ni_{26}Co_5Cr_2$	VIM; hot rolling (to 50 %) at 900 °C then homogenized at 1200 °C for 2 h then water quenched; cold rolled to 64 % reduction then homogenized at 900 °C for 10 min then water quenched	FCC	375; 645;760	58;58;17	[102]

$Fe_{50}Mn_{30}Co_{10}Cr_{10}$	VIM; hot rolling (to 50 %) at 900 ℃ then homogenized at 1200 ℃ for 2 h then water quenched; cold rolled to 50 % reduction then homogenized at 900 ℃ for 10 min then water quenched	FCC + HCP	730; 830; 870	75: 63; 50	[55]
$Fe_x(CoNi)_{90-x}Cr_{10}$ (x = 55, 57.5, 60 at. %)	VIM then homogenized at 1100 ℃ for 6 hr then pickled in 20 % HCl; cold rolled to 79 % reduction then homogenized at 800 ℃ for 10 min then water quenched	FCC + BCC	530-580	72-90	[160]
$Fe_{42}Ni_{19}Cr_{17}Co_{15}Al_4Zr_3$; $Fe_{41}Ni_{20}Cr_{18}Co_{10}Al_9Zr_2$	LPBF; then homogenized at 950 ℃ for 6 h then water quenched	FCC + BCC with $M_{23}Zr_6$ and M_xZr_y	1480-1600	20-18	[161]
$(FeNi)_{67}Cr_{15}Mn_{10}Al_{8-x}Ti_x$ (x = 3, 4 and 5 at. %)	VAM and then solution treated at 1150 ℃ for 2 h subsequently cold rolled 66 % then homogenized at 1150 ℃ for 2 min, water quenched, and finally aged at 800 ℃ for 1 h	FCC + γ' with η and $L2_1$ as precipitates	484-1247	65-23	[139]
$Al_{10}Cr_{15}(Fe_3Mn)_{75-x}Ni_x$ (x = 5 - 20 at. %)	VAM followed by 1100 ℃ for 2 h then water quenched	FCC + BCC/B2	600 - 800	60 - 26 %	[162]

$Fe_{50}Mn_{30}Co_{10}Cr_{10}Al_xTi_y$	SLM	FCC + HCP with TiAl as precipitates	78-854	15.5-31.8	[163]
$Fe_{25}Ni_{25}Co_{25}Ti_{15}Al_{10}$	MA + SPS	BCC and FCC with γ' and oxide	2520	5.2	[143]
$Fe_{50}Mn_{30}Co_{10}Cr_{10}$	GA + SPS	FCC + HCP	745	28.1	[119]
$Fe_{35}Ni_{35}Mn_{10}Cr_{20}C_{1.2}$	MA + SPS (at 500 °C to 1000 °C sintering temperature and 30 MPa pressure)	FCC with M_7C_3 carbide	180-1200	30-75	[64]
$Fe_{40}Mn_{40}Co_{10}Cr_{10}C_{3.3}$ with different cold rolled condition (5%, 11%, 14%, 18% and 22%)	Electromagnetic levitation melting	FCC	800-950	25-72	[63]
$(Fe_{32}Mn_{32}Ni_8Cr_8Al_{20})_{100-x}C_x$ (x = 0-2.5 at. %)	VAM	BCC + B2 (x <1 at. %), and FCC + $L2_1$/B2 (x >1 at. %)	1039-1128	15-42	[164]
$Fe_{46.4}Mn_{34.8}Ni_{11.3}Cr_6Al_{7.5}C_{0-1.1}$	VAM	FCC	535-1174	40.8-52.3	[106]
$Fe_2Ni_2CrAlC_x$ (x = 0-3.8 at. %)	VAM	FCC + BCC/B2	2392-2886	37.16-46.93	[165]
$Fe_{40.4}Ni_{11.3}Mn_{34.8}Al_{7.5}Cr_6C_{1.1}$	VAM	FCC with $M_{23}C_6$ and M_7C_3	750 MPa	52 %	[166]
$Fe_{34}Mn_{15}Ni_{11}Cr_{20}Co_{20}C_{0.5}$ and $Fe_{30}Cr_{20}Mn_{24}Co_{20}Ni_6C_{0.5}$	VIM followed by hot rolled at 950 °C with 50 % reduction then homogenized at 1200	FCC	402 and 646	40 and 36	[167]

	℃ for 2 h and water quenched				
Non-equiatomic Fe-Mn-Al-C and Fe-Mn-Al-Si-C	VIM followed by hot rolling at 1100 ℃ to reduction of 85 % then homogenized at 1100 ℃ for 30 min and air and water cooled	FCC	700-1110	56- 98	[60]
18Ni Maraging Steel	SLM	BCC + FCC	1800 MPa	6	[168]
Martensite and Ferrite DP steel	Casting followed by as-quench	BCC + HCP	920	22	[169]

1.6.2 Wear properties

The excellent wear properties of HEAs make them suitable for structural and biomaterial applications. Usually, materials with high hardness value shows good wear-resistance. HEAs are well known for high hardness. The wear properties are well established in the conventional alloys and HEAs but high entropy steel and Fe-based HEAs lacks sufficient experimental data. The wear properties of the FCC phase $Fe_{40.4}Ni_{11.3}Mn_{34.8}Al_{7.5}Cr_6$ with C doped high entropy steel were compared with 316L and Cantor alloy [170]. This high entropy steel showed less wear as compared to 316L and Cantor alloy. The better wear resistance was due to the stable and hard Al_2O_3 layer in high entropy steel [170]. Yu et al. [171] fabricated $(CoCrFeMnNi)_{100-x}C_x$ (x = 0–1.2 wt. %) HEAs using SPS have the FCC phase along with $M_{23}C_6$ and M_7C_3 type carbide. The presence of carbides helps to achieve high hardness and lower wear rate up to 3200 MPa and 1.59×10^{-4} mm^3 N^{-1} m^{-1}, respectively for 1.2 wt% C. The dominant wear mechanism in this alloy is oxidative, contact fatigue, and adhesive wear [171]. The microstructure of the Fe-based HEAs after laser claddings showed columnar dendrites with two crystalline structures of FCC and HCP [172]. Boron addition

(at 5.40 at. %) led to improve the wear rate by more than 30 % as compared with HEA without B content due to the formation of M_2B-type intermetallic [172]. Fe-based $Fe_{1.5}Al_{0.5}CrMnNi_{0.5}$ HEA was compared with commercially available alloys: 316, cast iron, Stellite 6, 17-4PH stainless steel [173]. The alloy showed the better wear resistance than that of Stellite 6, 316, and 17-4PH steel due to the formation of hard $Cr_5Fe_6Mn_8$ intermetallic in as-homogenized alloy [173]. Table 1.4 summarize the wear properties and their remedies or deterioration of various reported high entropy steels, Fe-based HEAs and non-equiatomic HEAs, which are prepared using various synthesis routes.

Table 1. 4: Wear properties and cause for improvement/deterioration in wear properties of the various reported high entropy steels, Fe-based HEAs, and non-equiatomic HEAs with different processing routes.

HEAs	Processing route	Phases	Wear properties	Reason for improvement in wear properties	Ref.
$Fe_{40.4}Ni_{11.3}Mn_{34.8}Al_{7.5}Cr_6$ doped with C	VIM	FCC	Superior wear resistance at as compared with 316L and Cantor HEA	The formation of harder Al_2O_3 oxide layer and it was stable	[170]
$Al_{0.5}CrFe_{1.5}MnNi_{0.5}$	VAM and aged at 700 ◦C for 10 h	FCC, BCC with TiC as precipitates	Superior wear resistance at room and high temperature	Hard B2 precipitates and formed the protective glazing layer	[174]
$Fe_4CoCrNiB_{0.2}Mo_x$	Thin film (Laser cladding) on Q235 steel	BCC + FCC with M_2B	Highest specific wear rate at x =1 at. %	Hard BCC phase, and grain size strengthening	[127]

$(FeCoNi)_{88-x}(AlTi)_{12}Mo_x$ (x = 0–1.5 at. %)	VAM	Dual FCC phase with gamma prime (γ')	Better wear rate (x = 1)	Due to formation of MoO_3	[175]
$(Fe_{0.25}Co_{0.25}Ni_{0.25}(B_{0.7}Si_{0.3})_{0.25})_{100-x}Nb_x$ (x = 0, 1, 2, 3, 4 at. %)	Thin film on 316L	FCC + BCC with Laves and (Fe, Co, Ni)$_2$B as precipitates	Firstly, by adding Nb wear resistance increased then decreased and superior wear resistance is showed by x = 2 at. %	High hardness due to presence of amorphous phase	[128]
$(CoCrFeMnNi)_{100-x}C_x$ (x = 0–1.2 wt. %)	SPS	FCC	Better wear rate (x = 1.2)	Due to the maximum amount of intermetallics presence (x = 1.2)	[171]
$Fe_{50}Mn_{30}Co_{10}Cr_{10}$ reinforced with graphene nanoplatelets	MA + SPS	FCC	Tribological properties improved by adding the reinforcement (0.2 wt %)	High hardness and self-lubricating capability of reinforcement	[176]
$Al_{0.2}Co_{1.5}CrFeNi_{1.5}Ti_{0.5+x}Si_x$ (x = 0.1–0.5, at. %)	SPS	Dual-phase with titanium silicides	Lowest wear rate (x = 0.5)	Due to the formation of titanium silicides and oxide	[177]

$Fe_{50-x}Mn_{30}Co_{10}Cr_{10}B_x$ (x = 0.1, 0.66 and 5.40 at. %)	Laser cladding	FCC + HCP with M_2B	5.40 at% B contain has the better wear resistance	Due to the presence of borides (max. phase fractions)	[172]

1.6.3 Functional properties

The promising functional properties of HEAs mainly include the electrical, magnetic, electrochemical, and biomaterial. The unexpected properties in the HEAs are achieved due to the cocktail effect [178]. The magnetic material mainly depends on the structural and microstructural, processing route and its parameters, composition, etc. Li et al., [179] prepared the $CoFe_2NiMn_{0.3}AlCu_x$ (x = 0.25, 0.50, 0.75, and 1.00 at. %) HEAs using VAM, and obtained the mixture of FCC and BCC phase solid solution. The saturation magnetization and coercivity of the alloys decreases as Cu content increases. The decrease in magnetic behaviour is due to the decrease in total concentrations of ferromagnetic element (Fe, Co, and Ni) and increase in Cu. Additionally, the weak bonding characteristics between the elements may happen because of the positive mixing enthalpy between Cu and other alloying elements [179].

The biomaterials require both mechanical properties i.e., good combination of strength and ductility, low elastic constant, better wear-resistant, and biocompatibility properties i.e., cytocompatibility and corrosion resistance in body fluids. HEAs shows excellent wear and corrosion resistance, good combination of strength and ductility, which makes them suitable for biomaterial applications. HEAs like TiNbTaZrHf, TiNbTaZrMo, TiNbTaZrW, TiNbTaZrFe, TiNbTaZrCr, have been reported with better biocompatibility than pure titanium, Ti-6Al-4V and 316L [180–182]. The outstanding biocompatible characteristics of HEAs along with excellent

mechanical properties, and wear and corrosion resistance, make them potential candidates for biomaterial application. The mechanical properties of various potential high entropy alloys for bioimplant applications, different bones and teeth are summarized in the Table 1.5.

Table 1.5: The mechanical properties for biomedical applications of HEAs as contrasted to hard tissues.

Sample designations	T.S. (MPa)	C.S. (MPa)	E.S. (GPa)	H (GPa)	Ref.
TiZrHfNbTa	---	800-985	80	---	[183]
TiZrNbTaMo	---	2600	---	4.9	[181, 182]
AlCrFeMnNi	---	1091-1200	---	5.3	[184]
AlCoCrFeNi	370	---	203	1.4	[185]
TiMoZrTaSi	---	800	69-89	3.8	[186]
AlCuSiZnFe	---	1987	279	6.67-9.55	[187]
$Co_{40}Cr_{16}Fe_{35}Ni_8Ti_1$	820-1200	---	---	---	[188, 189]
FeMoTaTiZr	---	---	108-129	5.5-10.2	[188, 190]
Cortical bone	35-283	88-164	10-30	0.43	[191, 192]
Cancellous bone	1.5-38	2-12	0.01-1.57	0.46	[191]
Human tooth (Enamel)	10	384	41.4	2.23-2.54	[192, 193]
Human tooth (Dentin)	52	295	18.6	3.3	[191, 194]
316L			210		[190]

1.7 Strengthening mechanisms

The arrangement of atoms in the metals and alloys is responsible for the strengthening mechanisms, and this naturally applies to HEAs. The major strengthening mechanisms are due to

grain size, precipitation, dislocation, and solid solution. The inherent strength comes from the internal frictional stress to dislocation motion, and further strength arises from various strengthening mechanisms. The yield strength of the alloy is due to the overall effect of frictional stress (σ_o), grain boundary (σ_{gb}), dislocation (σ_d), precipitation (σ_p) and solid solution strengthening (σ_{ss}). This can be expressed in the following equation, [195]

$$\sigma_y = \sigma_o + \sigma_{gb} + \sigma_d + \sigma_p + \sigma_{ss} \quad (1.9)$$

The solid solution strengthening, the first proposed model is the Fleischer model, which works on the assumption that the concentration of solute atoms is less and the HEAs are partitioned into two solutes i.e., one is taken as a whole solute matrix and the other remaining elements as solute element [196]. Mostly, this model is applicable for non-equiatomic HEAs by taking the assumption as pseudo dilute alloys. In $(FeCoNiCr)_{94}Ti_2Al_4$ and $FeCoNiCrT_{0.2}$ HEAs, the FeCoNiCr as a whole solute matrix and low-concentration elements are considered as solute elements [197, 198]. The solid solution strengthening of the alloy is calculated using the Fleischer model [199], which can be given as,

$$\sigma_{ss} = \frac{MG\varepsilon_f}{700} c^{\frac{1}{2}} \quad (1.10)$$

where, M = Taylor constant, G = shear modulus, c = percent of solute atom, and ε_f = relation parameter,

$$\varepsilon_f = \left| \frac{\varepsilon_G}{1+0.5|\varepsilon_G|} - 3\varepsilon_a \right|^{3/2} \quad (1.11)$$

where, atomic size misfit (a), $\varepsilon_a = \frac{1}{a}\frac{da}{dc}$ and modulus (G) mismatch, $\varepsilon_G = \frac{1}{G}\frac{dG}{dc}$.

The dislocations are inherently present in the crystalline alloys to a varying extent, which carry the plastic flow. The movement of dislocations interact from different slip planes with each other

in different ways, which are obstacles to one group of dislocation to another group. To overcome the mutual hindrance of dislocations in the alloys to move forward require higher applied stress as compared to ideal crystal. The contribution of dislocation strengthening in alloys increases as the dislocation density is higher. The dislocation strengthening is commonly described by the Taylor hardening model [200], as follows

$$\sigma_d = M\alpha Gb\sqrt{\rho_{dd}} \tag{1.12}$$

where, M = Taylor factor, G = Shear modulus, α = constant, ρ_{dd} = dislocation density, and b is the Burger's vector.

The grain boundary strengthening in HEAs arises due to obstructions of dislocation motion at grain boundaries. It is ascribed to two reasons; one is the dislocations motion in a particular direction is disrupted at grain boundaries, and secondly it is due to the incoherence of the slip plane from one grain to another [201, 202]. The grain boundary strengthening depends upon the average size of the grains. Coarse grains facilitate for more dislocation pile up in comparison with fine grains; this gives rise to high stress built up at grain boundary in case of coarse grain. So, yield strength is higher in case of fine-grained structure [203, 204]. The grain boundary strengthening was expressed by the Hall-Petch relationship [205, 206]. Mathematically,

$$\sigma_{gb} = k_y d^{-1/2} \tag{1.13}$$

where, k_y = slope of Hall-Petch and d = grain size diameter.

The precipitates are another hindrance for dislocation motion. The interaction between the precipitates and dislocations motions gives rise to another strengthening mechanism known as precipitation strengthening. The precipitation strengthening depends on precipitate size and the lattice coherency with the matrix. Firstly, the precipitate size is small and coherent with the matrix,

and then the dislocation moves forward by cutting through precipitates and is termed as particle shearing mechanism [207]. Secondly with larger precipitate size, Orowan by-pass mechanism is applied i.e., particle-dislocation interaction mechanism sets in, which glides through by-pass the precipitate particle [195, 207]. The precipitation strengthening by Orowan, manifested in the equation [50, 208],

$$\sigma_p = M\frac{0.4Gb}{\pi\lambda}\frac{\ln(\frac{2\bar{r}}{b})}{\sqrt{1-\upsilon}} \quad (1.14)$$

$$\lambda = 2\bar{r}(\sqrt{\frac{\pi}{4f}} - 1) \quad (1.15)$$

where, f = volume fraction of carbides, $\bar{r} = r\sqrt{\frac{2}{3}}$ is the mean radius of a circular cross-section, r = mean radius, and λ = distance between the precipitates. The HEAs are mainly precipitates strengthened by varying the composition and heat treatment. The common intermetallics formed in the HEAs are $L1_2$ (Ni_3Al-type) [209–211], B2 (NiAl-type) [212, 213], σ-type [214, 215], carbide precipitation [51, 216] and Laves-type [217, 218]. Some HEAs strengthened by precipitation are $Al_{7.5}Co_{20.5}Fe_{24}Ni_{24}Cr_{24}$ (FCC with $L1_2$ and B2-phase precipitates) [219], $(FeCoNi)_{81}Cr_9Al_8Ti_1Nb$ (FCC along with γ′ and B2-phase precipitates) [220], FeCoCrNiMn-1.3C HEA (FCC with $M_{23}C_6$ carbides precipitate) [208], $Al_{0.5}CrNbTi_2V_{0.5}$ (BCC with Laves phase precipitates) [221], and $(FeNi)_{67}Cr_{15}Mn_{10}Al_{8-x}Ti_x$ (x = 3, 4, and 5, at. %) (FCC+ γ' coexisted γ and η-phase precipitates) [139].

1.8 Application of High Entropy Steels and Fe-based HEAs

The unique compositional feature can induce various mechanical and functional properties in high entropy alloys. It makes them potential candidates for various applications. So, the various prospective applications in many scenarios have been mentioned:

- High-temperature applications: Excellent strength, wear and corrosion resistance at elevated temperatures, oxidation resistance, and creep resistance makes HEAs suitable for high temperature applications.
- Tool and hard-facing materials: HEAs are characterised by good strength, toughness, high hardness, impact strength, low wear resistance which are the requirements of a good tool material.
- Chemical plants: Better corrosion and wear resistance in harsh environments, and cavitation resistance make HEAs suitable to be used in chemical plant as well as in chemical piping systems.
- Light transportation materials: Excellent strength to weight ratio, good fatigue strength and creep resistance, and formability makes them for future light weight high strength material.
- Electric and magnetic materials: higher electrical resistivity and low eddy current loss, stable magnetization in larger temperature range make them potential candidate for soft magnetic and electric applications.
- Biomaterials: Low elastic modulus and density, high strength and ductility, better biocompatibility, excellent wear and corrosion resistance, these properties make them suitable candidate for biomaterial applications.
- Coating materials: improved hot hardness, high hardness, better scratch and wear resistance makes alloys used for future coating materials.

1.9 Motivation

It has been a major challenge for researchers to combine strength and ductility in a single material. High entropy alloy due to its compositional vastness has the flexibility to tune the structural and functional properties [24]. High entropy steel was designed and developed on the concept of HEAs, and it showed the combination of strength and ductility. Raabe et al. [60] first designed the FeMnAl-C and FeMnAlSi-C high entropy steels with major FCC phase. Though their alloys have average strength, they were able to achieve excellent tensile ductility (> 90 %) [60]. Our motivation is to design a low density dual-phase (FCC and BCC/B2) high entropy steel with nanoprecipitates which will enhance the mechanical properties. So firstly, we designed FeMnNiAlSiC high entropy steel, by adding Ni in the FeMnAlSiC high entropy steel to promote a secondary phase (B2). Then Ti and Cr are added to form nano carbides which will enhance strength and hardness. This would also improve wear resistance and biocompatibility. The majority of elements used here are low cost (Fe, Mn, Ni, Cr, Al, Si, and C) and low density (Al = 2.7 g/cc, Si = 2.33 g/cc, and Ti = 4.5 g/cc) elements.

$(FeNi)_{67}Cr_{15}Mn_{10}Al_{8-x}Ti_x$ HEAs forms the dual-phase structure of FCC and γ' (gamma prime) coexisted with η and $L2_1$ as nanoprecipitates by VAM [139]. They stated that Cr above 15 at. % will facilitate the formation of intermetallic compounds such as σ, μ, Laves, etc., whereas Mn above 10 at. % led to the formation of BCC phases. The design rationale is to fabricate low-density Fe-based HEAs with dual-phase structure with some precipitates. The addition of Al and Ti takes care of precipitation, and high Mn (around 20 at. %) should stabilize BCC phase. The effects of Ni and Cr on microstructure and mechanical properties of Fe-based HEAs were also studied systematically.

Powder metallurgy route is opted for the synthesis of high entropy steel and Fe-based HEAs due to the fact that mechanical alloying extends the solid solubility of elements and can promote homogenous and nanocrystalline structure. Consolidation of milled powder is done using SPS for retaining nanocrystalline structure.

1.10 Objective of the thesis

The primary objective of the work is to analyse the structural evolution, thermal stability, and mechanical properties of the high entropy steel and Fe-based HEAs. Further, the tribological properties and biocompatibility studies are done in the high entropy steel and Fe-based alloys. The mechanical properties of the present alloy systems are understood with the help of various strengthening mechanisms. The following objectives are mentioned as follows:

- To synthesise and study phase evolution of the high entropy steels and Fe-based HEAs during mechanical alloying.
- To study phase transformation of the high entropy steels and Fe-based HEAs after annealing and SPS.
- To model strengthening mechanisms to be correlated with the experimental yield strength of the high entropy steels and Fe-based HEAs.
- To design low-density high entropy steel and Fe-based HEAs, which may form the dual-phase structure along with the precipitates.
- To improve room temperature mechanical properties of the high entropy steels and Fe-based HEAs with an appreciable amount of ductility.
- To enhance wear resistance and biocompatibility of the high entropy steels and Fe-based HEAs by compositional variation.